Hindawi Publishing Corporation
Advances in High Energy Physics
Volume 2015, Article ID 641906, 10 pages
http://dx.doi.org/10.1155/2015/641906

Research Article

On Distributions of Emission Sources and Speed-of-Sound in Proton-Proton (Proton-Antiproton) Collisions

Li-Na Gao and Fu-Hu Liu

Institute of Theoretical Physics, Shanxi University, Taiyuan, Shanxi 030006, China

Correspondence should be addressed to Fu-Hu Liu; fuhuliu@163.com

Received 17 July 2015; Revised 5 November 2015; Accepted 19 November 2015

Academic Editor: Luca Stanco

The revised (three-source) Landau hydrodynamic model is used in this paper to study the (pseudo)rapidity distributions of charged particles produced in proton-proton and proton-antiproton collisions at high energies. The central source is assumed to contribute with a Gaussian function which covers the rapidity distribution region as wide as possible. The target and projectile sources are assumed to emit isotropically particles in their respective rest frames. The model calculations obtained with a Monte Carlo method are fitted to the experimental data over an energy range from 0.2 to 13 TeV. The values of the squared speed-of-sound parameter in different collisions are then extracted from the width of the rapidity distributions.

1. Introduction

In hadron-hadron, hadron-nucleus, and nucleus-nucleus (heavy ion) collisions at high energies, the final-state particles could be produced by multiple emission sources (which we denote also by fireballs) within the interacting system. This scenario can be tested by means of an analysis of the kinematic distributions of final-state particles. Proton-proton (proton-antiproton) collisions are usually used as a reference for the measurements in nucleus-nucleus collisions, in which the quark-gluon plasma (QGP) is expected to be formed [1]. From proton-proton collisions to nucleus-nucleus collisions, the distributions of emission sources may be similar to each other due to the small influences of nuclear effects such as the spectators and stopping power. The distributions of emission sources in high energy proton-proton (proton-antiproton) collisions can provide information on particle production in longitudinal rapidity and transverse momentum spaces.

In the study of distributions of emission sources, a principal question is whether there is a central source at midrapidity. If yes, what is the dependence of the relative contribution to particle production of the central source on collision energy? If no, what is the dependence of the width of the gap between two neighbouring sources around midrapidity on collision energy? In experiments at available accelerators and colliders, do the distributions of emission sources change with energy? Generally, common phenomenological models are useful in answering these questions. We focus on a few phenomenological models such as the three-fireball model [2–7], the three-source relativistic diffusion model [8–11], the multisource thermal model [12–14], the model with two Tsallis (or Boltzmann-Gibbs) clusters of fireballs [15–17], and the Landau hydrodynamic model [18–21] which results in a Gaussian shape for the rapidity distribution [21, 22] and a few revised versions such as works of Gao and Liu [23], Wong [24], Jiang et al. [25–30], Beuf et al. [31], and Bialas et al. [32].

The three-fireball model [2–7] assumes the nucleon to be an extended object and to consist of valence quarks, sea quarks, and gluons. The interacting system formed in high energy proton-proton collisions can be divided into three fireballs: a central fireball located at midrapidity, a target fireball located in the backward (target) rapidity region, and a projectile fireball located in the forward (projectile) rapidity region. The three-source relativistic diffusion model [8–11] was also proposed to have three fireballs or sources: a central source located at midrapidity and arising from interactions between low-momentum gluons in both target and projectile, a target-like source located in the backward

rapidity region and arising from interactions between valence quarks in the target and low-momentum gluons in the projectile, and a projectile-like source located in the forward rapidity region and arising from interactions between low-momentum gluons in the target and valence quarks in the projectile.

The multisource thermal model [12–14] is the successor of the thermalized cylinder model and the two-cylinder model. The thermalized cylinder model was proposed to have a (central) thermalized cylinder at midrapidity and two leading nucleon sources in target and projectile rapidity regions, respectively. The two-cylinder model uses two (target/projectile) cylinders and two leading (target/projectile) nucleon sources. In the case of the two cylinders having a gap between them, there is no source at midrapidity. In most cases, there are sources at midrapidity due to the two cylinders overlapping each other or having no gap between them. In the model with two Tsallis clusters of fireballs [15], the rapidity distributions are described by using a superposition of two Tsallis fireballs along the rapidity axis. In the energy range from 0.5 to 7 TeV, the model result [15] shows that there is a gap between the two clusters, and there is no source at midrapidity. The Tsallis clusters can be replaced by others such as the Boltzmann-Gibbs clusters [16, 17].

The Landau hydrodynamic model [18–21] uses only a central source at midrapidity. The rapidity distribution obtained in the model is simply a Gaussian function [21, 22] in which the width is related to the speed-of-sound. A few revised versions were proposed in literature [22–32] to give better descriptions for experimental data, some of which include the contributions of leading and nonleading nucleons. We focus on a simple revised version [23] in which a central source at midrapidity, a target source in the backward rapidity region, and a projectile source in the forward rapidity region are used. In the simple revised version, the central source is assumed to contribute with a Gaussian function which covers the rapidity distribution region as wide as possible. The target and projectile sources are assumed to emit isotropically particles in their respective rest frames.

From the above introduction, we see that most models were proposed to have a central source at midrapidity. In particular, under the assumption that the emitting sources are thermalized fireballs, the width of the rapidity distribution obtained by the (revised) Landau hydrodynamic model can be used to extract the squared speed-of-sound parameter, which is related to the mean free path of the strongly interacting particles in the sources in the central, forward, and backward rapidity regions. We use the simple revised Landau hydrodynamic model [23] to describe the (pseudo)rapidity distribution. Because the widths of rapidity distributions obtained from the central source and from the target (or projectile) source are different, we expect to extract different values of the squared speed-of-sound parameter for the central and target (or projectile) sources.

In view of the wider application of the Landau hydrodynamic model [18–22] and its various revisions [22, 24–32], we have used the simple revised (three-source) Landau hydrodynamic model to study the pseudorapidity and rapidity distributions of charged particles produced in symmetric and asymmetric nuclear collisions at high energies in our recent work [23]. As a follow-up paper of [23], this work focuses on proton-proton (and proton-antiproton) collisions and presents a more detailed description of the model and its implementation. The definition of kinetic quantities is the same as in [23] according to universal representations, in order to provide a consistent picture.

In this paper, we use the simple revised (three-source) Landau hydrodynamic model to study the pseudorapidity and rapidity distributions of charged particles produced in proton-proton (proton-antiproton) collisions at high energies. In Section 2, a description of the model and calculation method is presented. Both pseudorapidity and rapidity distributions are obtained separately [33]. In Section 3, the pseudorapidity distributions are compared with the experimental data of proton-proton (proton-antiproton) collisions over an energy range from 0.2 to 13 TeV [34–42]. The values of the squared speed-of-sound parameter are then extracted from the width of the rapidity distributions. In Section 4, we summarize our main observations and conclusions.

2. The Revised Landau Hydrodynamic Model and Calculation Method

The first 1+1-dimensional hydrodynamic model was proposed by Landau many years ago [18]. Later, a complex analytical solution was obtained by Khalatnikov [19]. The rapidity distribution of charged particles obtained from the complex analytical solution by Belenkij and Landau is [20]

$$\frac{dN_{\mathrm{ch}}}{dy} \propto \exp\left(\sqrt{L^2 - y^2}\right), \tag{1}$$

where $L = \ln(\sqrt{s_{NN}}/2m_p)$ is the logarithmic Lorentz contraction factor, $\sqrt{s_{NN}}$ denotes the center-of-mass energy per pair of nucleons, and m_p denotes the rest mass of a proton. A later study [21] showed that the rapidity distribution of charged particles follows a Gaussian function

$$\frac{dN_{\mathrm{ch}}}{dy} \propto \exp\left(-\frac{y^2}{2L}\right) \tag{2}$$

in the case of $L \gg |y|$.

The second 1+1-dimensional hydrodynamic model and its analytical solution were obtained by Hwa [43] in the limit of $\sqrt{s_{NN}} \to \infty$. A plateau structure in rapidity distribution was obtained, which departs from available experimental results. Based on Hwa's work, Bjorken obtained the energy density of particles in high energy collisions [44]. By taking into account the contributions of leading particles and based on a theory of unified description of Hwa-Bjorken and Landau relativistic hydrodynamics, pseudorapidity distributions of charged particles in agreement with the experimental results were obtained in a recent work [23]. For the central source,

the unified hydrodynamic model describes the rapidity distribution of charged particles to be [22]

$$\frac{dN_{\mathrm{ch}}}{dy} = C\frac{|y|}{\left[\left(\theta_{\mathrm{FO}} - \sqrt{\theta_{\mathrm{FO}}^2 - c_s^2 y^2}\right)\left(\theta_{\mathrm{FO}}^2 - c_s^2 y^2\right)\right]^{1/2}} \cdot \exp\left[-\frac{1-c_s^2}{2c_s^2}\left(\theta_{\mathrm{FO}} - \sqrt{\theta_{\mathrm{FO}}^2 - c_s^2 y^2}\right)\right], \tag{3}$$

where C is the normalization constant, c_s^2 is the squared speed-of-sound, $\theta_{\mathrm{FO}} = \ln(T_0/T_k)$, T_0 denotes the initial temperature, and T_k denotes the kinetic freeze-out temperature.

Equation (3) is similar to a Gaussian distribution [22]

$$\frac{dN_{\mathrm{ch}}}{dy} = \frac{N_0}{\sqrt{2\pi}\sigma}\exp\left[-\frac{(y-y_C)^2}{2\sigma^2}\right], \tag{4}$$

where N_0 is the normalization constant, σ is the distribution width, and y_C is the midrapidity. In symmetric collisions, $y_C = 0$ in the center-of-mass reference frame. In our simple revised version of the Landau hydrodynamic model [23], σ should be large enough to cover the rapidity region as wide as possible. The relation between c_s^2 and σ can be given by [18, 24, 45–49]

$$\sigma = \sqrt{\frac{8}{3}\frac{c_s^2}{1-c_s^4}L}. \tag{5}$$

Then, c_s^2 is expressed by using σ to be

$$c_s^2 = \frac{1}{3\sigma^2}\left(\sqrt{16L^2 + 9\sigma^4} - 4L\right). \tag{6}$$

To perform the calculation for (pseudo)rapidity distribution as accurately as possible, we need also the transverse momentum (p_T) distribution. Here we use the simplest Boltzmann distribution [50]

$$f_{p_T}(p_T) = C_0 p_T \exp\left(-\frac{\sqrt{p_T^2 + m_0^2}}{kT_B}\right), \tag{7}$$

where C_0 is the normalization constant, k denotes the Boltzmann constant, T_B is the effective temperature which is larger than the kinetic freeze-out temperature T_k, and m_0 denotes the rest mass of the considered particle. The chemical potential and the distinction for fermions and bosons are not included due to small effects on transverse momentum distribution at high energy. Equation (7) means that we assume thermal emission of the final-state particles.

We introduce the transverse momentum distribution in the model so that we can obtain rapidity and pseudorapidity separately. In fact, to convert between rapidity and pseudorapidity distributions, additional limit is needed. The Boltzmann distribution describes the most fraction of the transverse momentum distribution. Equation (7) is not the sole choice for the transverse momentum distribution. In fact, we can also use other choices such as the Tsallis distribution [51, 52], the Tsallis form of standard distribution [53, 54], and the Erlang distribution [55]. In the study of rapidity or pseudorapidity distribution, the form of (7) and the value of parameter in it are not sensitive factors. Instead, the distributions of emission sources influence largely the rapidity or pseudorapidity distribution.

In the simple revised version of the Landau hydrodynamic model, we use in fact three sources: a central (C) source described by (4) and (7), a target (T) source described by an isotropic emission picture and (7), and a projectile (P) source equal to the target source. The central source describes the contributions of all produced particles, partly nonleading nucleons, and all leading nucleons, while the target and projectile sources describe the contributions of partly nonleading nucleons. In the rapidity space, the central source stays at midrapidity y_C and the target (projectile) source stays at rapidity y_T (y_P) in the backward (forward) target (projectile) region.

We used a Monte Carlo method to perform the calculation for the central source. Let $R_{1,2,3}$ denote random numbers in $[0, 1]$. According to (4) and (7), we have $y = \sigma\sqrt{-2\ln R_1}\cos(2\pi R_2) + y_C$ and $\int_0^{p_T} f_{p_T}(p_T)dp_T < R_3 < \int_0^{p_T+dp_T} f_{p_T}(p_T)dp_T$, respectively. The longitudinal momentum is $p_z = \sqrt{p_T^2 + m_0^2}\sinh y$, the momentum $p = \sqrt{p_T^2 + p_z^2}$, and the pseudorapidity

$$\eta = \frac{1}{2}\ln\left(\frac{p+p_z}{p-p_z}\right). \tag{8}$$

In the calculation for the target and projectile sources, particles are assumed to be emitted isotropically in their respective rest frames. In the Monte Carlo method, the emission angle is as follows:

$$\theta' = \arctan\left[\frac{2\sqrt{R_4(1-R_4)}}{1-2R_4}\right] + \theta_0, \tag{9}$$

where $\theta_0 = 0$ (or π) in the case of the first term in the above equation being larger than 0 (or smaller than 0) and R_4 denotes a random number in $[0, 1]$. This isotropic emission results approximately in a Gaussian pseudorapidity distribution with the width of 0.91–0.92 [56], which can be compared with the theory of unified description of Hwa-Bjorken and Landau relativistic hydrodynamics [22], in which the rapidity of particle is assumed to obey a Gaussian distribution with the width of 0.85. In the present work, we do not need to study further the width corresponding to the target and projectile sources due to the fixed value of 0.91.

The transverse momentum p_T of the particle produced in the target or projectile source has the same expression as those in the central source. The longitudinal momentum $p_z' = p_T\cot\theta'$, the momentum $p' = \sqrt{p_T^2 + p_z'^2}$, and the energy $E' = \sqrt{p'^2 + m_0^2}$ in the rest frame of the considered

source can be extracted. In the laboratory or center-of-mass reference frame, the rapidity y is given by

$$y = \frac{1}{2}\ln\left(\frac{E' + p'_z}{E' - p'_z}\right) + y_{T,P}. \quad (10)$$

The longitudinal momentum p_z, the momentum p, and the pseudorapidity η have the same expressions as those for the central source.

In the above discussions, the rapidity distribution, $dN_{\rm ch}/dy$, and the pseudorapidity distribution, $dN_{\rm ch}/d\eta$, can be obtained separately, where $N_{\rm ch}$ denotes the multiplicity of charged particles.

3. Comparisons with Experimental Data and Discussion

The pseudorapidity distributions, $dN_{\rm ch}/d\eta$, of charged particles produced in proton-proton (p-p) collisions at $\sqrt{s_{NN}}$ =0.2, 0.41, 0.9, 2.36, 7, and 13 TeV are presented in Figure 1, where $\sqrt{s_{NN}}$ is simplified to $\sqrt{s}$ for proton-proton and proton-antiproton collisions. The squares represent the experimental data measured by the PHOBOS [34] ((a), (b)), ALICE [35, 36] ((c), (d), (g)), and CMS [37, 38] ((e), (f), (h)) Collaborations, whereas the curves represent our model results calculated by means of the Monte Carlo method. The types of collisions, inelastic interactions (INEL) or nonsingle diffractive interactions (NSD), are marked in the panels. We take $m_0 = 0.174\,\text{GeV}/c^2$ for the central source and $m_0 = 0.938\,\text{GeV}/c^2$ for the target and projectile sources, respectively. The former is estimated from an average of the weighted masses and yields of $\pi^{\pm}$, $K^{\pm}$, $\overline{p}$, and p [57]; the latter is the mass of a proton due to protons being the charged particles in the target (projectile) source.

The effective temperature T_B in (7) is taken to be 0.156 GeV [58, 59], which is the value extracted from a statistical hadronization model (a Grand-Canonical thermal model) analysis of lead-lead collisions at 2.76 TeV. This value is the chemical freeze-out temperature which can be extended to nucleus-nucleus collisions over an energy range from the critical energy (the minimum center-of-mass energy required to reach the phase transition to the QGP, which is thought to be in the range 10–20 GeV [58, 59]) to TeV and shows decrease for decreasing $\sqrt{s_{NN}}$. The energy range (0.2–13 TeV) considered in the present work is above the critical energy. As a small system, the collision discussed in the present work should have a chemical freeze-out temperature $T_{\rm ch}$ which is less than 0.156 GeV. As the kinetic freeze-out temperature, T_k should be lower than $T_{\rm ch}$, due to final-state elastic rescattering of the hadrons. And as the effective temperature in (7), T_B is larger than T_k, due to the effect of radial flow. It is hard to say the relative size between T_B and 0.156 GeV, due to $T_B > T_k < T_{\rm ch} < 0.156$ GeV. We assume T_B to be 0.156 GeV and independent of energy in 0.2–13 TeV. In the fits for the rapidity and pseudorapidity distributions, T_B is not a very sensitive quantity, and a relative large (~10%) increase or decrease in T_B does not cause a very obvious change in the distributions. As an example, the dotted and dashed curves in Figure 1(h) are the fits with $1.1T_B$ (≈0.172 GeV) and $0.9T_B$ (≈0.140 GeV), respectively.

The values of the peak position y_T and relative contribution k_T of the target source, the rapidity distribution width σ of the central source, the normalization constant N_0, and χ^2 per degree of freedom (χ^2/dof) fitted by the method of least squares are given in Table 1, together with the squared speed-of-sound $c_s^2(T)$ for the target source and the squared speed-of-sound $c_s^2(C)$ for the central source. For p-p collision, the peak position y_P and relative contribution k_P of the projectile source, the peak position y_C and the relative contribution k_C of the central source, and the squared speed-of-sound $c_s^2(P)$ for the projectile source are given by $y_P = -y_T$, $k_P = k_T$, $y_C = 0$, $k_C = 1 - k_T - k_P$, and $c_s^2(P) = c_s^2(T)$, respectively.

Figure 2 is similar to Figure 1, but it shows the results in proton-antiproton (p-$\overline{p}$) collisions at $\sqrt{s} = 0.54$, 0.63, 0.9, and 1.8 TeV. The solid squares and curves represent the experimental data measured by the UA1 [39] (a), CDF [40] ((b), (f)), P238 [41] (c), and UA5 [42] ((d), (e)) Collaborations and our model results, respectively, and the open squares are reflected at $\eta = 0$. The obtained values of y_T, k_T, σ, χ^2/dof, $c_s^2(T)$, and $c_s^2(C)$ are given in Table 1. The relations among different peak positions, relative contributions, and speeds of sound for p-$\overline{p}$ collision are the same as those for p-p collision.

Figures 1 and 2 show that the model results describe the experimental data. In the considered energy range, (i) y_T does not show an obvious dependence on the energy $\sqrt{s}$, or y_T for p-p (p-$\overline{p}$) collision has a slight decrease (increase) with increase of $\sqrt{s}$; (ii) k_T does not show an obvious change with $\sqrt{s}$; (iii) σ increases with increase of $\sqrt{s}$; (iv) $c_s^2(T) < c_s^2(C)$, and they are clearly flat as functions of $\sqrt{s}$.

To see clearly the dependence of y_T, σ, $c_s^2(T)$, and $c_s^2(C)$ on $\sqrt{s}$, we plot the parameter values listed in Table 1, in Figure 3. The symbols and lines represent the parameter values and linear fitting functions, respectively. The intercepts, slopes, and χ^2/dof corresponding to the lines in Figure 3 are listed in Table 2. The conclusions obtained from Figure 1, Figure 2, and Table 1 can be also seen in Figure 3.

In the above discussions, the physics picture and calculation method are the same as our previous work [23] which deals with symmetric and asymmetric nuclear collisions and is different from our other works [60, 61] in which four sources (target/projectile participant sources and target/projectile spectator sources) are used. In the present work, we have used a large enough central source which is described by the Landau hydrodynamic model [18–22] and two small target and projectile sources which revise the model. The rapidity range covered by the two participant sources is the same as that of the three fireballs [2–7] or three sources [8–11], and the two spectator sources are beyond the scope of the compared picture, due to the former appearing in very backward or forward region. The rapidity range covered by the central source in the revised Landau hydrodynamic model is the same as that of the compared picture, and the target/projectile sources appear in the scope of the central source.

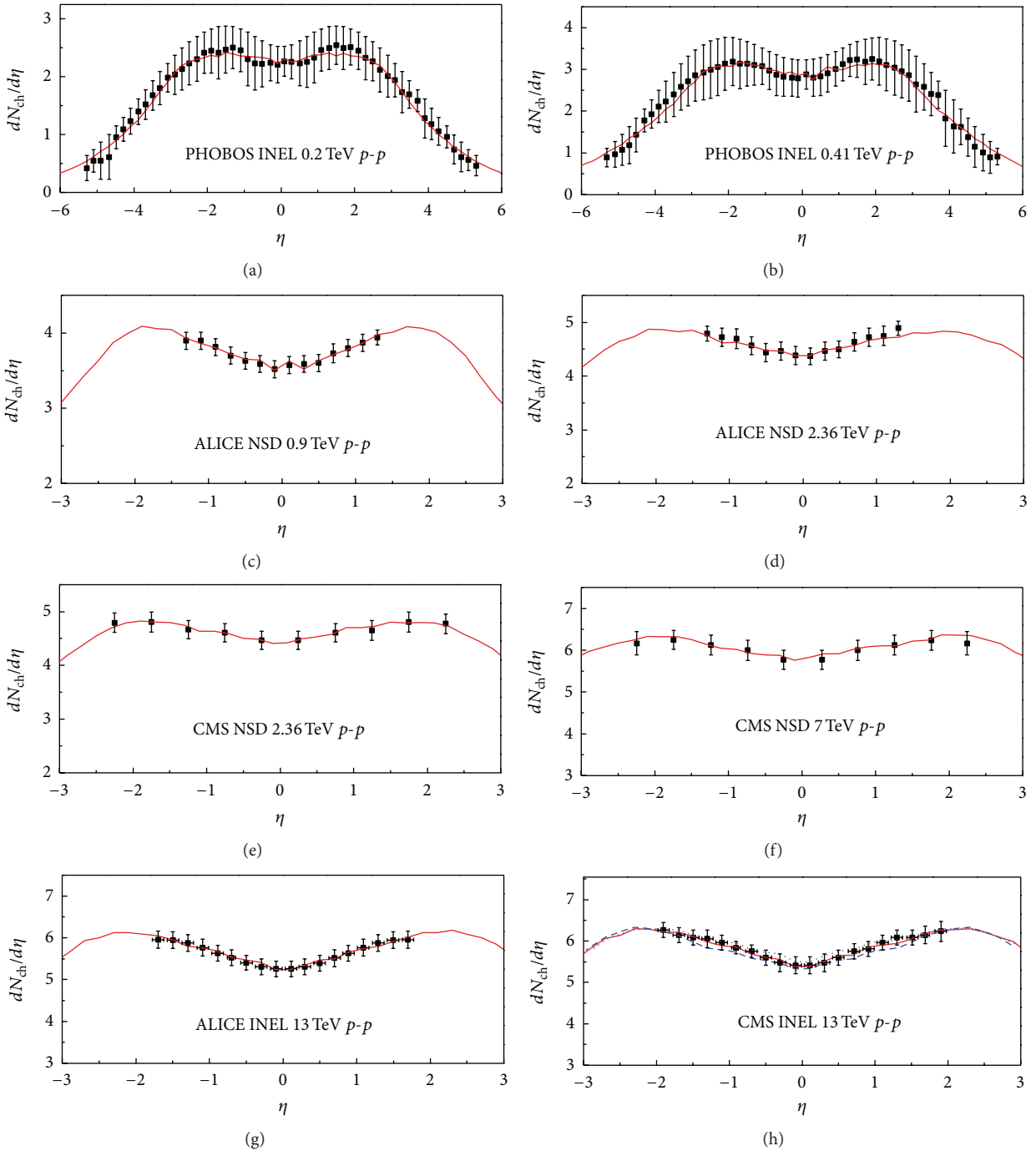

FIGURE 1: Pseudorapidity distributions of charged particles produced in p-p collisions at high energies. The squares represent the experimental data of the PHOBOS [34] ((a), (b)), ALICE [35, 36] ((c), (d), (g)), and CMS [37, 38] ((e), (f), (h)) Collaborations, whereas the curves represent our fitted results.

Because different methods are used, the present work obtains a different $c_s^2(C)$ (≈1/3~1/2) from our previous works [60, 61] (≈0.15~0.28). We observe that the new revised Landau hydrodynamic model yields larger values of $c_s^2(C)$. Let D denote the dimensionality of space. We have the relation $c_s^2 = 1/D$ for massless particles [62, 63]. Then, the value $c_s^2 = 1/3$ for $D = 3$ corresponds to the ideal gas state (large mean free path) of hadronic matter investigated by different groups in the past [64–68] and more recently [69–73]; instead, $c_s^2 = 1/2$ for $D = 2$ corresponds to the ideal liquid state (small mean free path) investigated by Buchbinder et al. [63]. The present work seems to suggest that the target and projectile sources formed in proton-proton (proton-antiproton) collisions at $\sqrt{s} = 0.2$–13 TeV stay in

Table 1: Fitted values of y_T, k_T, σ, N_0, and χ^2/dof corresponding to the curves in Figures 1 and 2 which show the pseudorapidity distributions in p-p and p-$\overline{p}$ collisions at different energies. The last two columns show $c_s^2(T)$ and $c_s^2(C)$.

Figure	$\sqrt{s}$ (TeV)	y_T	k_T	σ	N_0	χ^2/dof	$c_s^2(T)$	$c_s^2(C)$
Figure 1(a)	0.2	−1.85 ± 0.17	0.027 ± 0.012	2.75 ± 0.02	20.50 ± 0.37	0.207	0.066 ± 0.010	0.472 ± 0.050
Figure 1(b)	0.41	−1.73 ± 0.12	0.020 ± 0.008	3.15 ± 0.07	29.20 ± 0.43	0.221	0.057 ± 0.009	0.511 ± 0.050
Figure 1(c)	0.9	−1.23 ± 0.12	0.027 ± 0.008	3.03 ± 0.02	35.00 ± 0.68	0.007	0.050 ± 0.008	0.446 ± 0.050
Figure 1(d)	2.36	−1.72 ± 0.05	0.016 ± 0.007	3.37 ± 0.03	47.80 ± 0.52	0.013	0.043 ± 0.006	0.467 ± 0.016
Figure 1(e)	2.36	−1.71 ± 0.06	0.013 ± 0.010	3.32 ± 0.04	47.00 ± 0.50	0.003	0.043 ± 0.006	0.458 ± 0.020
Figure 1(f)	7	−2.16 ± 0.13	0.020 ± 0.008	3.50 ± 0.06	65.80 ± 0.83	0.009	0.038 ± 0.006	0.447 ± 0.010
Figure 1(g)	13	−1.76 ± 0.02	0.026 ± 0.006	3.63 ± 0.06	63.20 ± 0.42	0.008	0.035 ± 0.001	0.447 ± 0.010
Figure 1(h)	13	−1.78 ± 0.03	0.024 ± 0.005	3.66 ± 0.04	65.30 ± 0.38	0.011	0.035 ± 0.001	0.452 ± 0.006
Figure 2(a)	0.54	−1.32 ± 0.17	0.020 ± 0.002	2.44 ± 0.02	12.80 ± 0.27	0.070	0.055 ± 0.001	0.347 ± 0.040
Figure 2(b)	0.63	−1.70 ± 0.05	0.050 ± 0.003	3.05 ± 0.01	33.00 ± 0.64	0.466	0.053 ± 0.001	0.468 ± 0.050
Figure 2(c)	0.63	−2.70 ± 0.24	0.010 ± 0.003	3.30 ± 0.09	33.70 ± 0.49	0.192	0.053 ± 0.001	0.516 ± 0.050
Figure 2(d)	0.9	−0.85 ± 0.03	0.012 ± 0.005	3.08 ± 0.04	33.00 ± 0.63	0.028	0.050 ± 0.001	0.456 ± 0.050
Figure 2(e)	0.9	−0.80 ± 0.08	0.023 ± 0.007	3.12 ± 0.03	29.50 ± 0.58	0.070	0.050 ± 0.001	0.464 ± 0.050
Figure 2(f)	1.8	−1.75 ± 0.08	0.050 ± 0.002	3.10 ± 0.03	20.90 ± 0.33	0.784	0.045 ± 0.001	0.428 ± 0.040

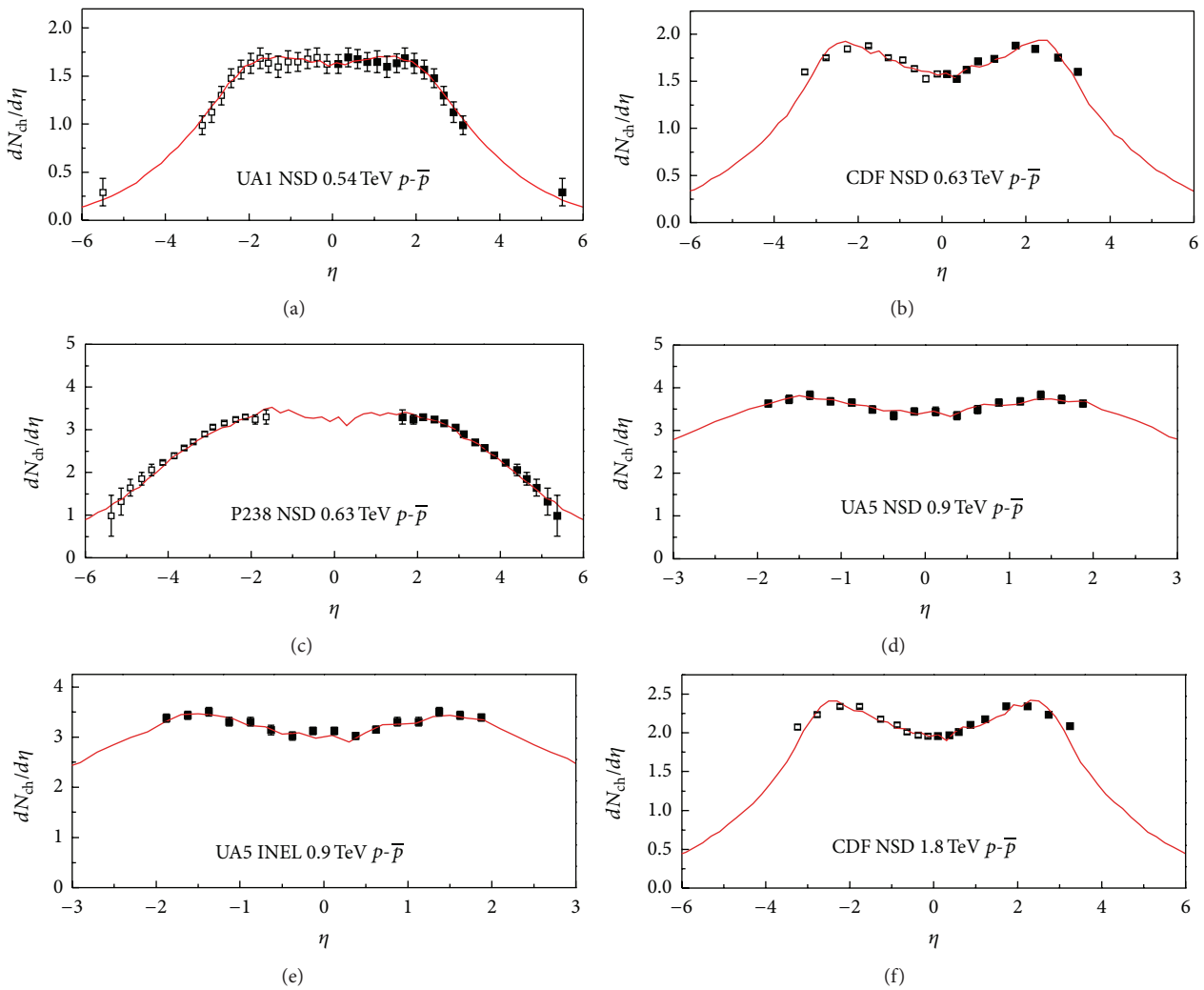

Figure 2: Pseudorapidity distributions of charged particles produced in p-$\overline{p}$ collisions at high energies. The solid squares and curves represent the experimental data of the UA1 [39] (a), CDF [40] ((b), (f)), P238 [41] (c), and UA5 [42] ((d), (e)) Collaborations and our fitted results, respectively, and the open squares are reflected at $\eta = 0$ due to symmetry.

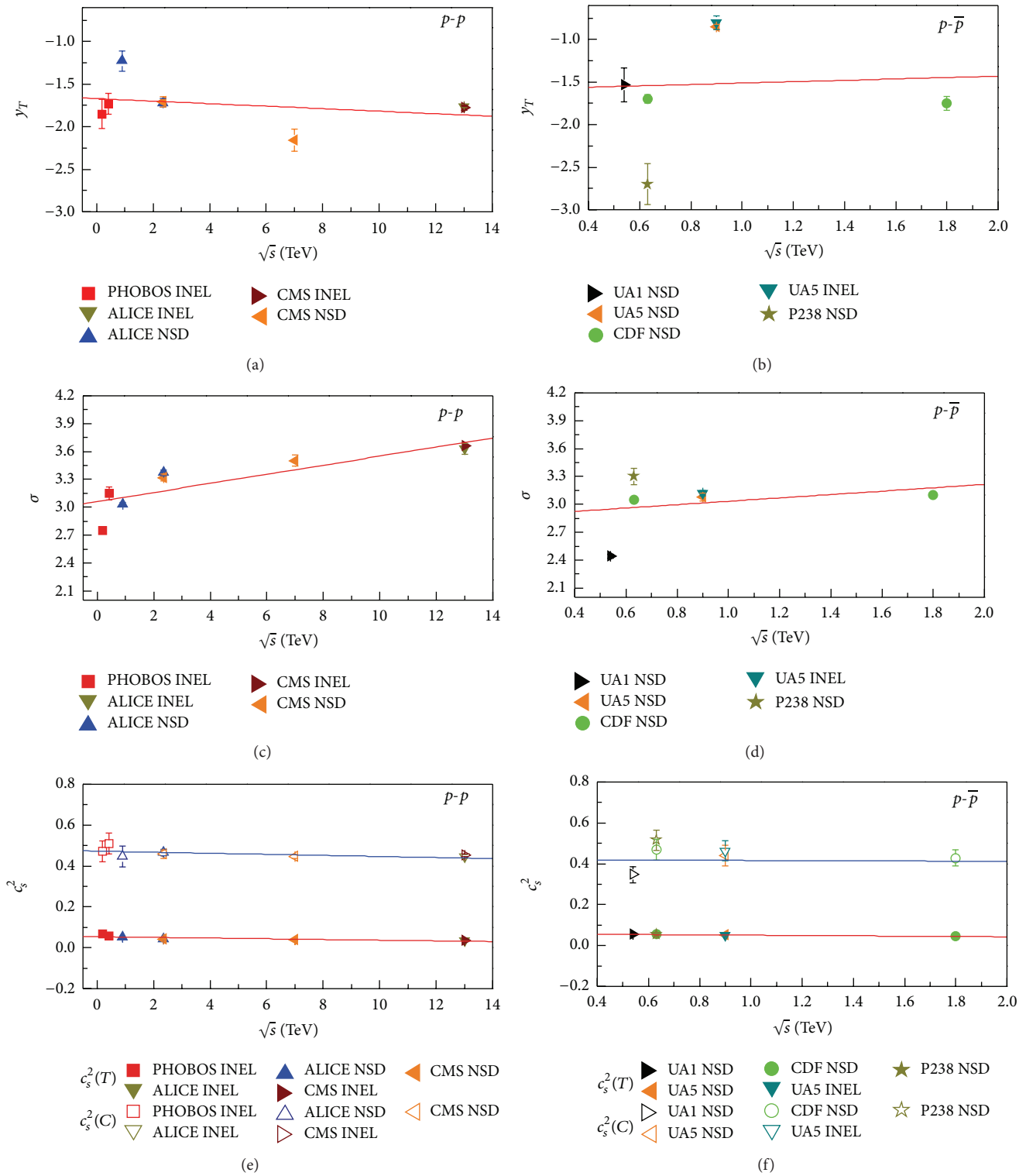

FIGURE 3: Collision energy dependence of y_T ((a), (b)), σ ((c), (d)), $c_s^2(T)$ ((e), (f)), and $c_s^2(C)$ ((e), (f)) for p-p ((a), (c), (e)) and p-$\overline{p}$ ((b), (d), (f)) collisions. The symbols represent the values of free parameters and squared speed-of-sound listed in Table 1. The lines are our fitted results, though some of them do not obey linear relations.

Table 2: Values of intercept, slope, and χ^2/dof corresponding to the linear fits in Figure 3, though some of them do not obey linear relations. The unit of $\sqrt{s}$ is TeV.

Figure	Type	Intercept	Slope	χ^2/dof
Figure 3(a)	$y_T - \sqrt{s}$	-1.670 ± 0.118	-0.015 ± 0.017	9.697
Figure 3(b)	$y_T - \sqrt{s}$	-1.593 ± 0.673	0.081 ± 0.676	157.282
Figure 3(c)	$\sigma - \sqrt{s}$	3.061 ± 0.080	0.049 ± 0.011	55.317
Figure 3(d)	$\sigma - \sqrt{s}$	2.852 ± 0.270	0.182 ± 0.271	188.858
Figure 3(e)	$c_s^2(T) - \sqrt{s}$	0.054 ± 0.003	-0.002 ± 0.001	3.657
	$c_s^2(C) - \sqrt{s}$	0.473 ± 0.009	-0.003 ± 0.001	1.159
Figure 3(f)	$c_s^2(T) - \sqrt{s}$	0.058 ± 0.001	-0.007 ± 0.001	1.054
	$c_s^2(C) - \sqrt{s}$	0.451 ± 0.054	-0.005 ± 0.054	2.179

the gas-like state and the central source stays in a liquid-like state. However, the QGP is an extended system in which colour confinement is removed (partonic degrees of freedom) and local thermal equilibrium is reached. In small collision systems, like proton-proton and proton-antiproton, the large values of $c_s^2(C)$ cannot be interpreted as a parameter of an extended thermalized system.

4. Conclusions

We summarize here our main observations and conclusions.

(a) As in nucleus-nucleus collisions, the interacting system formed in proton-proton (proton-antiproton) collisions can be also divided into three emission sources. The central source is large enough to cover the whole (pseudo)rapidity region and is described by the Landau hydrodynamic model. The small target (projectile) source which is isotropic in its rest frame is used to revise the Landau hydrodynamic model and the (pseudo)rapidity distribution. Our treatment of the distributions of emission sources is a revision of the Landau hydrodynamic model. The model calculations obtained with a Monte Carlo method can describe the experimental data of proton-proton and proton-antiproton collisions over an energy range from 0.2 to 13 TeV.

(b) In proton-proton and proton-antiproton collisions in the considered energy range, the free parameters and the squared speed-of-sound c_s^2 do not show an obvious dependence on the energy. The values of $c_s^2(C)$ extracted for the central source are in the range from 1/3 to 1/2, and the values of $c_s^2(T)$ for the target and projectile sources are in the range from 0.04 to 0.07. It is interesting to note that the values of $c_s^2(C)$ in the range of 1/3 to 1/2 are expected to characterize the formation of a QGP in high energy collisions of heavy nuclei. The interpretation of large $c_s^2(C)$ in small systems such as in proton-proton and proton-antiproton collisions remains an open question that deserves further investigation.

Conflict of Interests

The authors declare that there is no conflict of interests regarding the publication of this paper.

Acknowledgments

This work was supported by the National Natural Science Foundation of China under Grant no. 11575103, the Open Research Subject of the Chinese Academy of Sciences Large-Scale Scientific Facility under Grant no. 2060205, the Shanxi Provincial Natural Science Foundation under Grant no. 2013021006, and the Shanxi Scholarship Council of China under Grant no. 2012-012.

References

[1] T. D. Lee and G. C. Wick, "Vacuum stability and vacuum excitation in a spin-0 field theory," *Physical Review D*, vol. 9, no. 8, pp. 2291–2316, 1974.

[2] A. D'Innocenzo, G. Ingrosso, and P. Rotelli, "A new two-component model for *pp* topological gross-sections," *Il Nuovo Cimento A*, vol. 44, no. 3, pp. 375–391, 1978.

[3] A. D'innocenzo, G. Ingrosso, and P. Rotelli, "The $p\overline{p}$ annihilation channel as a prototype for the central fireball in *pp* production processes," *Lettere al Nuovo Cimento*, vol. 25, no. 13, pp. 393–398, 1979.

[4] A. D'Innocenzo, G. Ingrosso, and P. Rotelli, "A universal scaling function for hadron-hadron interactions," *Il Nuovo Cimento A*, vol. 55, no. 4, pp. 417–436, 1980.

[5] A. D'Innocenzo, G. Ingrosso, and P. Rotelli, "The three-component fireball model and $p\overline{p}$ interactions," *Lettere Al Nuovo Cimento*, vol. 27, no. 14, pp. 457–466, 1980.

[6] L.-S. Liu and T.-C. Meng, "Multiplicity and energy distributions in high-energy e^+e^-, pp, and $p\overline{p}$ collisions," *Physical Review D*, vol. 27, no. 11, pp. 2640–2647, 1983.

[7] C. Kuang-Chao, L. Lian-Sou, and M. Ta-Chung, "Koba-Nielsen-Olesen scaling and production mechanism in high-energy collisions," *Physical Review D*, vol. 28, no. 5, pp. 1080–1085, 1983.

[8] G. Wolschin, "Relativistic diffusion model," *The European Physical Journal A*, vol. 5, no. 1, pp. 85–90, 1999.

[9] G. Wolschin, "Diffusion in relativistic systems," *Progress in Particle and Nuclear Physics*, vol. 59, no. 1, pp. 374–382, 2007.

[10] G. Wolschin, "Pseudorapidity distributions of produced charged hadrons in pp collisions at RHIC and LHC energies," *EPL*, vol. 95, no. 6, Article ID 61001, 2011.

[11] G. Wolschin, "Particle production sources at LHC energies," *Journal of Physics G*, vol. 40, no. 4, Article ID 045104, 2013.

[12] F.-H. Liu, "Particle production in Au-Au collisions at RHIC energies," *Physics Letters, Section B: Nuclear, Elementary Particle and High-Energy Physics*, vol. 583, no. 1-2, pp. 68–72, 2004.

[13] F.-H. Liu, "Dependence of charged particle pseudorapidity distributions on centrality and energy in p(d)A collisions at high energies," *Physical Review C*, vol. 78, no. 1, Article ID 014902, 2008.

[14] F.-H. Liu, "Unified description of multiplicity distributions of final-state particles produced in collisions at high energies," *Nuclear Physics A*, vol. 810, no. 1–4, pp. 159–172, 2008.

[15] L. Marques, J. Cleymans, and A. Deppman, "Description of high-energy pp collisions using Tsallis thermodynamics: transverse momentum and rapidity distributions," *Physical Review D*, vol. 91, no. 5, Article ID 054025, 2015.

[16] F. Becattini and J. Cleymans, "Chemical equilibrium in heavy ion collisions: rapidity dependence," *Journal of Physics G: Nuclear and Particle Physics*, vol. 34, no. 8, pp. S959–S963, 2007.

[17] J. Cleymans, "Rapidity and energy dependence of thermal parameters," *Journal of Physics G*, vol. 35, no. 4, Article ID 044017, 2008.

[18] L. D. Landau, "Izvestiya akademii nauk: series fizicheskikh 17 51 (1953)," in *English-Translation: Collected Papers of L. D. Landau*, D. Ter-Haarp, Ed., p. 569, Pergamon, Oxford, UK, 1965.

[19] I. M. Khalatnikov, "Some questions of the relativistic hydrodynamics," *Journal of Experimental and Theoretical Physics*, vol. 27, pp. 529–541, 1954 (Russian).

[20] S. Z. Belenkij and L. D. Landau, "Soviet Physics Uspekhi 56 309 (1955)," in *English-Translation: Collected Papers of L.D. Landau*, D. Ter-Haarp, Ed., p. 665, Pergamon, Oxford, UK, 1965.

[21] P. A. Steinberg, "Bulk dynamics in heavy ion collisions," *Nuclear Physics A*, vol. 752, no. 1–4, pp. 423–432, 2005.

[22] Z. J. Jiang, H. P. Deng, Y. Zhang, and H. L. Zhang, "Unified descriptions of Hwa-Bjorken and Landau relativistic hydrodynamics and the pseudorapidity distributions in high energy heavy ion collisions," *Nuclear Physics Review* (Chinese), In press.

[23] L.-N. Gao and F.-H. Liu, "On pseudorapidity distribution and speed of sound in high energy heavy ion collisions based on a new revised Landau hydrodynamic model," *Advances in High Energy Physics*, vol. 2015, Article ID 184713, 23 pages, 2015.

[24] C.-Y. Wong, "Landau hydrodynamics reexamined," *Physical Review C*, vol. 78, no. 5, Article ID 054902, 2008.

[25] Z. J. Jiang, Q. G. Li, and H. L. Zhang, "Revised Landau hydrodynamic model and the pseudorapidity distributions of charged particles produced in nucleus-nucleus collisions at maximum energy at the BNL Relativistic Heavy Ion Collider," *Physical Review C*, vol. 87, no. 4, Article ID 044902, 2013.

[26] Z. J. Jiang, K. Ma, H. L. Zhang, and L. M. Cai, "Pseudorapidity distributions of the produced charged particles in nucleus-nucleus collisions at low energies at the BNL relativistic heavy ion collider," *Chinese Physics C*, vol. 38, no. 8, Article ID 084103, 2014.

[27] H. L. Zhang and Z. J. Jiang, "Investigations for energy dependences of pseudorapidity distributions of charged particles in p+p collisions," *Nuclear Physics Review*, vol. 31, pp. 8–13, 2014 (Chinese).

[28] Z. J. Jiang, H. L. Zhang, J. Wang, and K. Ma, "The evolution-dominated hydrodynamic model and the pseudorapidity distributions in high energy physics," *Advances in High Energy Physics*, vol. 2014, Article ID 248360, 10 pages, 2014.

[29] Z. J. Jiang, H. L. Zhang, K. Ma, and J. Wang, "A description of pseudorapidity distributions in p-p collisions at center-of-mass energy from 23.6 to 900 GeV," *Chinese Physics C*, vol. 39, no. 4, Article ID 044102, 2015.

[30] Z. J. Jiang, J. Wang, H. L. Zhang, and K. Ma, "Evolution-dominated hydrodynamic model and the pseudorapidity distributions of the charged particles produced in Cu-Cu collisions at BNL-RHIC energies," *Nuclear Physics Review*, vol. 31, pp. 460–467, 2014 (Chinese).

[31] G. Beuf, R. Peschanski, and E. N. Saridakis, "Entropy flow of a perfect fluid in (1+1) hydrodynamics," *Physical Review C*, vol. 78, no. 6, Article ID 064909, 2008.

[32] A. Bialas, R. A. Janik, and R. Peschanski, "Unified description of Bjorken and Landau 1+1 hydrodynamics," *Physical Review C*, vol. 76, no. 5, Article ID 054901, 2007.

[33] F.-H. Liu, Y.-H. Chen, Y.-Q. Gao, and E.-Q. Wang, "On current conversion between particle rapidity and pseudorapidity distributions in high energy collisions," *Advances in High Energy Physics*, vol. 2013, Article ID 710534, 4 pages, 2013.

[34] B. Alver, B. B. Back, M. D. Baker et al., "Charged-particle multiplicity and pseudorapidity distributions measured with the PHOBOS detector in Au+Au, Cu+Cu, d+Au, and p+p collisions at ultrarelativistic energies," *Physical Review C*, vol. 83, no. 2, Article ID 024913, 2011.

[35] K. Aamodt, N. Abel, U. Abeysekara et al., "Charged-particle multiplicity measurement in proton-proton collisions at $\sqrt{s}$ = 0.9 and 2.36 TeV with ALICE at LHC," *The European Physical Journal C*, vol. 68, pp. 89–108, 2010.

[36] J. Adam, D. Adamová, M. M. Aggarwal et al., "Pseudorapidity and transverse-momentum distributions of charged particles in proton-proton collisions at $\sqrt{s}$ = 13 TeV," *Physics Letters B*, In press.

[37] V. Khachatryan, A. M. Sirunyan, A. Tumasyan et al., "Transverse-momentum and pseudorapidity distributions of charged hadrons in *pp* collisions at $\sqrt{s}$ = 7 TeV," *Physical Review Letters*, vol. 105, Article ID 022002, 2010.

[38] V. Khachatryan, A. M. Sirunyan, A. Tumasyan et al., "Pseudorapidity distribution of charged hadrons in proton-proton collisions at $\sqrt{s}$ = 13 TeV," *Physics Letters B*, vol. 751, pp. 143–163, 2015.

[39] G. Arnison, A. Astbury, B. Aubert et al., "Charged particle multiplicity distributions in proton-antiproton collisions at 540 GeV center of mass energy," *Physics Letters B*, vol. 123, pp. 108–114, 1983.

[40] F. Abe, D. Amidei, G. Apollinari et al., "Pseudorapidity distributions of charged particles produced in $\overline{p}p$ collisions at $\sqrt{s}$ = 630 and 1800 GeV," *Physical Review D*, vol. 41, pp. 2330–2333, 1990.

[41] R. Harr, C. Liapis, P. Karchin et al., "Pseudorapidity distribution of charged particles in $\overline{p}p$ collisions at $\sqrt{s}$ = 630 GeV," *Physics Letters B*, vol. 401, pp. 176–180, 1997.

[42] G. J. Alner, R. E. Ansorge, B. Åsman et al., "Scaling of pseudorapidity distributions at c.m. energies up to 0.9 TeV," *Zeitschrift für Physik C*, vol. 33, no. 1, pp. 1–6, 1986.

[43] R. C. Hwa, "Statistical description of hadron constituents as a basis for the fluid model of high-energy collisions," *Physical Review D*, vol. 10, no. 7, pp. 2260–2268, 1974.

[44] J. D. Bjorken, "Highly relativistic nucleus-nucleus collisions: the central rapidity region," *Physical Review D*, vol. 27, no. 1, pp. 140–151, 1983.

[45] E. V. Shuryak, "Multiparticle production in high energy particle collisions," *Yadernaya Fizika*, vol. 16, no. 2, pp. 395–405, 1972.

[46] O. V. Zhirov and E. V. Shuryak, "Multiple production of hadrons and predictions of the Landau theory," *Yadernaya Fizika*, vol. 21, pp. 861–867, 1975.

[47] P. Carruthers and M. Duong-Van, "Rapidity and angular distributions of charged secondaries according to the hydrodynamical model of particle production," *Physical Review D*, vol. 8, no. 3, pp. 859–874, 1973.

[48] P. Carruthers, "Heretical models of particle production," *Annals of the New York Academy of Sciences*, vol. 229, no. 1, pp. 91–123, 1974.

[49] M. Gazdzicki, M. Gorenstein, and P. Seyboth, "Onset of deconfinement in nucleus-nucleus collisions: review for pedestrians

and experts," *Acta Physica Polonica B*, vol. 42, no. 2, pp. 307–351, 2011.

[50] C.-R. Meng, "Transverse momentum and rapidity distributions of φ mesons produced in Pb-Pb collisions at SPS energies," *Chinese Physics Letters*, vol. 26, no. 10, Article ID 102501, 2009.

[51] C. Tsallis, "Possible generalization of Boltzmann-Gibbs statistics," *Journal of Statistical Physics*, vol. 52, no. 1-2, pp. 479–487, 1988.

[52] C. Tsallis, "Nonadditive entropy and nonextensive statistical mechanics—an overview after 20 years," *Brazilian Journal of Physics*, vol. 39, no. 2, pp. 337–356, 2009.

[53] J. Cleymans and D. Worku, "Relativistic thermodynamics: transverse momentum distributions in high-energy physics," *The European Physical Journal A*, vol. 48, article 160, 2012.

[54] F. H. Liu, Y. Q. Gao, and H. R. Wei, "On descriptions of particle transverse momentum spectra in high energy collisions," *Advances in High Energy Physics*, vol. 2014, Article ID 293873, 12 pages, 2014.

[55] Y.-Q. Gao, C.-X. Tian, M.-Y. Duan, B.-C. Li, and F.-H. Liu, "Transverse momentum distributions of identified particles produced in pp, $p(d)A$, and AA collisions at high energies," *Pramana*, vol. 79, no. 6, pp. 1407–1423, 2012.

[56] M. I. Adamovich, M. M. Aggarwal, Y. A. Alexandrov et al., "Charged particle density distributions in Au induced interactions with emulsion nuclei at 10.7A GeV," *Physics Letters B*, vol. 352, pp. 472–478, 1995.

[57] A. Adare, S. Afanasiev, C. Aidala et al., "Spectra and ratios of identified particles in Au+Au and d+Au collisions at $\sqrt{s_{NN}}$ = 200 GeV," *Physical Review C*, vol. 88, Article ID 024906, 2013.

[58] A. Andronic, P. Braun-Munzinger, and J. Stachel, "Thermal hadron production in relativistic nuclear collisions: the hadron mass spectrum, the horn, and the QCD phase transition," *Physics Letters B*, vol. 673, pp. 142–145, 2009, Erratum in *Physics Letters B*, vol. 678, p. 516, 2009.

[59] J. Stachel, A. Andronic, P. Braun-Munzinger, and K. Redlich, "Confronting LHC data with the statistical hadronization model," *Journal of Physics: Conference Series*, vol. 509, no. 1, Article ID 012019, 2014.

[60] L.-N. Gao, Y.-H. Chen, H.-R. Wei, and F.-H. Liu, "Speed of sound parameter from RHIC and LHC heavy-ion data," *Advances in High Energy Physics*, vol. 2013, Article ID 450247, 8 pages, 2013.

[61] Y.-Q. Gao, T. Tian, L.-N. Gao, and F.-H. Liu, "Pseudorapidity distribution of charged particles and square speed of sound parameter in p-p or p-$\overline{p}$-collisions over an energy range from 0.053 to 7 TeV," *Advances in High Energy Physics*, vol. 2014, Article ID 569079, 9 pages, 2014.

[62] K.-Y. Kim and I. Zahed, "Baryonic response of dense holographic QCD," *Journal of High Energy Physics*, vol. 2008, no. 12, article 075, 2008.

[63] E. I. Buchbinder, A. Buchel, and S. E. Vázquez, "Sound waves in (2+1) dimensional holographic magnetic fluids," *Journal of High Energy Physics*, vol. 2008, no. 12, article 090, 2008.

[64] B. Betz, *Jet propagation and Mach-cone formation in (3+1)-dimensional ideal hydrodynamics [Ph.D. thesis]*, University Frankfurt, Frankfurt, Germany, 2009, http://arxiv.org/abs/0910.4114.

[65] P. M. Hohler and M. A. Stephanov, "Holography and the speed of sound at high temperatures," *Physical Review D*, vol. 80, no. 6, Article ID 066002, 2009.

[66] C. P. Herzog and S. S. Pufu, "The second sound of SU(2)," *Journal of High Energy Physics*, vol. 2009, no. 4, article 126, 2009.

[67] A. Cherman, T. D. Cohen, and A. Nellore, "Bound on the speed of sound from holography," *Physical Review D*, vol. 80, no. 6, Article ID 066003, 2009.

[68] U. Gürsoy, E. Kiritsis, L. Mazzanti, and F. Nitti, "Deconfinement and gluon plasma dynamics in improved holographic QCD," *Physical Review Letters*, vol. 101, no. 18, Article ID 181601, 2008.

[69] P. Castorina, J. Cleymans, D. E. Miller, and H. Satz, "The speed of sound in hadronic matter," *The European Physical Journal C*, vol. 66, no. 1, pp. 207–213, 2010.

[70] V. Roy and A. K. Chaudhuri, "Equation of state dependence of Mach cone-like structures in Au+Au collisions," *Journal of Physics G*, vol. 37, no. 3, Article ID 035105, 2010.

[71] S. K. Ghosh, T. K. Mukherjee, M. G. Mustafa, and R. Ray, "QGP susceptibilities from PNJL model," *Indian Journal of Physics*, vol. 85, no. 1, pp. 87–91, 2011.

[72] A. Bazavov, T. Bhattacharya, C. DeTar et al., "The equation of state in (2 + 1)-flavor QCD," *Physical Review D*, vol. 90, Article ID 094503, 2014.

[73] U. Heinz, P. Sorensen, A. Deshpande et al., "Exploring the propertiesof the phases of QCD matter—research opportunities and priorities for the next decade," http://arxiv.org/abs/1501.06477v2.